Eur. Phys. J. B **31**, 167–177 (2003)
DOI: 10.1140/epjb/e2003-00021-y

THE EUROPEAN PHYSICAL JOURNAL B

Electronic structure calculations of Fe-rich ordered and disordered Fe-Al alloys

E. Apiñaniz[1,a], F. Plazaola[2], and J.S. Garitaonandia[3]

[1] Elektrika eta Elektronika Saila, Zientzi Fakultatea, Euskal Herriko Unibertsitatea UPV- EHU, 644PK Bilbao, Spain
[2] Elektrika eta Elektronika Saila, Zientzi Fakultatea, Euskal Herriko Unibertsitatea UPV- EHU, 644PK Bilbao, Spain
[3] Dpto. Física Aplicada II, Facultad de Ciencias, Universidad del País Vasco UPV-EHU Apdo. 644 Bilbao, Spain

Received 7 May 2002 / Received in final form 20 September 2002
Published online 4 February 2003 –

Abstract. Tight Binding Linear Muffin-Tin Orbital (TB-LMTO) electronic calculations are presented for the magnetic and structural properties of ordered and disordered FeAl alloys. The total energy, bulk modulus, lattice parameter and magnetic moments of B2, D03 and B32 ordered structures and A2 disordered structure were calculated for different compositions. The different structures are obtained by varying the position of Fe and Al atoms in a BCC superstructure. In this way, we examine the order-disorder transition that takes place in these alloys. Disordered alloys present both larger Fe magnetic moment and lattice parameter than ordered ones. In this work comparison of the calculated quantities with available experimental results is provided and it can be concluded that the results are in quantitative agreement with the experimental trends.

PACS. 71.15.Ap Basis sets (plane-wave, APS, LCAO, etc.) and related methodology (scattering methods, ASA, linearized methods) – 71.15.Dx Computational methodology (Brillouin zone sampling, iterative diagonalization, pseudopotential construction) – 71.15.Nc Total energy and cohesive energy calculations – 71.20.Lp Intermetallic compounds

1 Introduction

The critical magnetic behaviour of Fe-based magnetic systems has been a subject of numerous theoretical and experimental investigations over the past two decades [1]. Iron and aluminium are mixable over the whole concentration range and show a very complex phase diagram [2]. As far as the structure is concerned the Fe rich side of the phase diagram of the Fe-Al system is characterised by a range of disordered body centred cubic (BCC) solutions up to 19 at.% Al at room temperature. On increasing the Al content, the phase diagram shows a variety of intermetallic phases such as $Fe_{13}Al_3$, Fe_3Al and FeAl. Starting with Al dissolved in Fe, the first stable structure is the D03 cubic structure and it exists over the 23−37 at.% Al range. The other stable compound existing over a wide range of composition is FeAl which is also cubic with the B2 structure (CsCl) and it exists over the range of 37−50 at.% Al. A new type of order in the iron rich part has also been reported, for a single crystal specimen of 20 at.% Al content, which has been slowly cooled (from 740 °C down to room temperature). In 1990 a B32 long-range order was observed with neutron-scattering experiments [3,4] and it is thought that the B32 phase has a tendency to exist at even larger deviations from stoichiometry than the B2 phase.

It has been shown that these alloys are of the ferromagnetic disordered type (BCC, A2) for Al composition up to 23 at.% independent of heat treatment [5]. In alloys with Al content ranging from 0 to about 30 at.% Al, the iron atoms carry their normal magnetic moment of 2.2 μ_B when they have at least five or more iron atoms as nearest neighbours [6–10]. It is thought that around that Al content the average magnetic moment per Fe atom decreases rapidly from 2.0 to 0.7 μ_B [5]. Above this composition (30 at.% Al) this alloy is paramagnetic at room temperature.

In addition, disordering the alloy can induce paramagnetic-ferromagnetic transitions. Over a period of time a variety of explanations to these transitions were proposed [6,10–13]. However, X-ray diffraction of ball milled alloys of $Fe_{60}Al_{40}$ composition shows an increase of the lattice parameter with milling time [14,15]. This increase has been assumed to produce a variation of the

[a] e-mail: eaf@we.lc.ehu.es

DOS at the Fermi level that would cause the magnetic transition [14–16].

Even though many band calculations have been used to study TM aluminides during the last years (for reviews on electronic-structure-calculation results of TM aluminides see references [17–19]), there are relatively few calculations aimed to the study of the influence of defects on the electronic and magnetic structure of TM aluminides. Haydock *et al.* [20] used LCAO (Linear Combinations of Atomic Orbitals) to determine the role of the local environment in determining the sizes of the magnetic moments in Fe_3Al. The LMTO method has been applied to study the electronic structure of antisite (AS) defects in FeAl where the point defect was modelled by suitably chosen supercells [21]. The LMTO-CPA technique has been used to discuss the order-disorder transition in FeAl alloys [22]. The supercell approach has been used in order to study the antiphase boundary in NiAl and FeAl [23] as well as point defects in these aluminides [24]. The onset of magnetism in Fe-Al system as a function of the defect structure was studied using the CPA within the KKR method for the disordered case and the TB-LMTO for the intermetallic compound [25], where they found appearance of large local magnetic moments associated to the Fe antisite defect.

The aim of this work is to study the magnetic properties and the large increase of magnetism in the order-disorder transition of the Fe-Al system. In order to reach this goal different structures (B2, D03, B32 and A2) present in the Fe-Al phase diagram were built for different Fe compositions and the ground-state properties for the lattice parameters that correspond to the minimum of the total energy at 0 K were calculated. On the other hand, the influence of the volume change on the magnetic properties is also studied.

2 Theoretical calculations

The conventional LMTO-ASA method [26,27], as well as its transformation to a localised representation TB-LMTO [28], are well described in the literature, therefore only the relevant computational details are given here. Both the von Barth and Hedin parameterisation for the local spin-density approximation [29] and the non-localised Perdew and Wang approximation for the exchange-correlation potential were used. The obtained data were compared with the available experimental results and it was found that the von Barth and Hedin local density functional is a good approximation for these calculations (see Tab. 2). In this work the latter have been used, because it gives a good estimate of the magnetic moments while the Perdew and Wang non-local approximation overestimates them. As it happens for the ground state properties of Fe [30], the lattice parameters obtained with the Perdew and Wang approximation are closer to the experimental ones.

The equation of state has been obtained by fitting the results with Murnaghan's equation [31]. The DOS

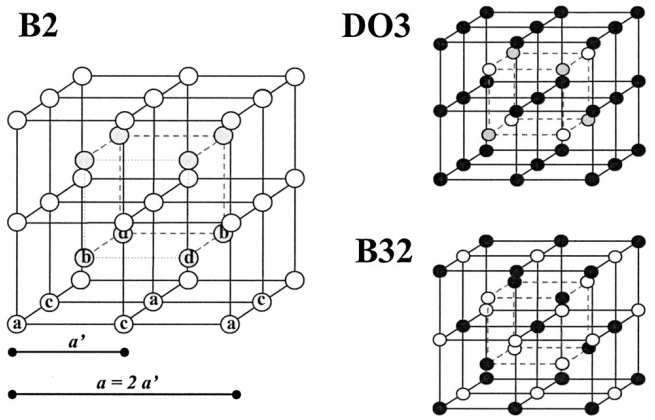

Fig. 1. The main structures of the Fe-rich side of the Fe-Al phase diagram. In the first picture the cell is divided in four different subcells (a, b, c and d) as described by Schmidt and Binder [34] (see text). Different colours mean different concentrations of Fe.

(Density of States) has been solved by the Tetrahedron integration method [32,33].

Even though for most of the structures 32 768 k-points have been used, we have noticed that the results between calculations done with 4 096 and 32 768 k-points are very close. Therefore in order to save CPU time, for structures with many non-equivalent atoms ($Fe_{81.25}Al_{18.75}$, $Fe_{87.5}Al_{12.5}$, A2-$Fe_{50}Al_{50}$ and A2-$Fe_{75}Al_{25}$) 32 768 k-points have been used only for the equilibrium lattice parameter. For the largest lattice cells (32 atom-cells) used to simulate the disorder 64 lattice points have been used.

Schmidt and Binder [34] gave a description of the main structures appearing in the Fe rich side of the phase diagram (see Fig. 1). Within this description, the different structures are simulated using a 16-atom unit cell that is divided into four subcells (a, b, c and d). Varying the concentration ratio between subcells gives the different structures corresponding to the Fe-rich side of the phase diagram. Using x_i^j as the concentration of each sublattice, where j is the type of atom (Al or Fe) and i the sublattice (for a binary alloy the relations for x_{Al} follow the same law as the ones for x_{Fe}), the simulated structures fulfil the following conditions:

a) B2 structure: $[x_{\mathrm{a}}^{\mathrm{Fe}} = x_{\mathrm{b}}^{\mathrm{Fe}}] \neq [x_{\mathrm{c}}^{\mathrm{Fe}} = x_{\mathrm{d}}^{\mathrm{Fe}}]$.
b) DO3 structure: $x_{\mathrm{a}}^j = x_{\mathrm{c}}^j$, $x_{\mathrm{b}}^j \neq x_{\mathrm{d}}^j$.
c) B32 phase: $[x_{\mathrm{a}}^j = x_{\mathrm{b}}^j] \neq [x_{\mathrm{c}}^j = x_{\mathrm{d}}^j]$.
d) Disordered A2 structure: $x_{\mathrm{a}}^j = x_{\mathrm{b}}^j = x_{\mathrm{c}}^j = x_{\mathrm{d}}^j$.

For the B2 structure $Fe_{50}Al_{50}$ the unit cell is half the unit cell of the other structures, but for comparison we double it in most sections of this paper.

The A2 structures have been simulated for $Fe_{75}Al_{25}$ and $Fe_{50}Al_{50}$ compositions. There are many configurations that fulfil the condition of the A2 structure shown before, and to simulate the disorder properly a cell as large as possible should be built, but when increasing the number of atoms the computational time also increases. Therefore three different cells with 16 atoms and four with 32 atoms

Table 1. Summary of the results for ordered and disordered structures. a is the lattice parameter, B is the Bulk modulus, μ_{Fe} (μ_{B}) is the magnetic moment per iron atom and E_{cohe} is the cohesive energy. E_{min} is the total energy at the equilibrium volume. The values in brackets correspond to non-polarized calculations.

Composition	Structure	a (a.u.)	B (Gpa)	μ_{Fe} (μ_{B})	E_{cohe} (eV)	E_{min} (eV)
$Fe_{50}Al_{50}$	B2	10.74 (10.77)	200	0.64	–5.91	–3743.302 (–3743.301)
	D03	10.93 (10.82)	173	1.71	–5.66	–3743.258 (–3743.240)
	B32	10.91 (10.82)	44	1.67	–5.73	–3743.270 (–3743.244)
$Fe_{75}Al_{25}$	B2	10.6 (10.50)	192	1.07	–6.25	–4086.982 (–4086.966)
	D03	10.65 (10.51)	176	1.86	–7.62	–4086.984 (–4086.969)
	B32	10.71	190	1.97	–6.18	–4086.913
$Fe_{81.25}Al_{18.75}$	D03	10.63 (10.47)	197	1.90	–6.31	–4153.892 (–4153.871)
$Fe_{87.5}Al_{12.5}$	B32	10.62 (10.43)	208	2.02	–6.38	–4215.130 (–4215.101)
$Fe_{50}Al_{50}$	A2	10.95 (10.83)	153	1.69	–5.5855	–3743.245 (–3743.234)
$Fe_{75}Al_{25}$	A2	10.72 (10.53)	193	2.00	–6.150	–4086.968 (–4086.947)

were built for each composition, which takes reasonable computational time. Afterwards the mean value was calculated and it can be seen that the results obtained for different cells are very close.

3 Results and discussion

3.1 Ordered structures

In order to study the evolution of the properties of these alloys with lattice parameter, alloys with different Fe and Al content and different structures have been studied. Besides, the study will help in understanding the influence of the nearest neighbourhood of Fe sites on the magnetic properties in different structures. Table 1 shows the results of our calculations in the different structures simulated for each composition and Table 2 presents the comparison between the experimental values of $Fe_{75}Al_{25}$ and $Fe_{50}Al_{50}$ compositions with the theoretical ones performed by different authors for the structures and compositions shown in the phase diagram. Moreover, one has to take into account that in FeAl alloys, depending on the thermal treatment, it is possible to find B2 and D03 phases in samples with the same composition [35], even if the phase diagram shows only a definite phase for that composition. Taking this point of view into account calculations of different structures for the same composition are also interesting.

3.1.1 $Fe_{50}Al_{50}$

Table 2 shows clearly that the different structural and magnetic parameters calculated for the B2 structure and $Fe_{50}Al_{50}$ composition are in very good agreement with previous calculations appearing in the literature [25,36].

Even though the energy for the spin-polarized calculations is lower, the energy difference for the equilibrium lattice parameter of the non-polarized and spin-polarized calculations is within the error (∼0.01 eV) that can be obtained with this method; therefore, we cannot conclude whether this structure is magnetic or not.

Figure 2a shows a jump of the mean magnetic moment per iron atom close to the equilibrium lattice parameter (spin-polarized calculations). The jump goes from zero to around 0.6 μ_{B}. Figure 2a shows the variation of the magnetic moment *versus* lattice parameter in the B2 structure of $Fe_{50}Al_{50}$. This phenomenon can be explained by taking into account the DOS (see Fig. 3a) and the difference between the majority and minority spin sub-bands. Gu *et al.* [21] show hybridisation of *sp*-Al and *d*-Fe bands in FeAl alloys. The hybridisation leads to charge transfer from Al to Fe atoms. The hybridisation makes the bandwidth increase, *i.e.* if there is hybridisation of *sp*-bands with *d*-bands there will be an increase of the width of these bands. Moreover, Heine [37] gives a relationship between the bandwidth and the hybridisation. Therefore in order to study the hybridisation phenomena that take place in these alloys the bandwidth parameter (Δ) obtained by the LMTO code is used. The LMTO code, to take into account hybridisation, writes the Hamiltonian with hoping integrals factorised into potential parameters (which specify the bandwidth) and screened structure constants [38]. The decrease of the lattice parameter induces an increase on the hybridisation (see the narrowing of the bandwidth with lattice-parameter increase in Tab. 3).

The hybridisation causes charge transfer between the majority and minority spin sub-bands. This makes the difference of the number between occupied states decrease and therefore, the magnetism of the alloy decreases.

Table 2. Comparison of different parameters of $Fe_{50}Al_{50}$ and $Fe_{75}Al_{25}$ compositions obtained in the present work for the phase-diagram structures with previous experimental and theoretical results. a_{exp} and a_{theo} are the experimental and theoretical lattice parameters, B_{exp} and B_{theo} are the experimental and theoretical Bulk modulus, μ_{theo} and μ_{exp} are the theoretical and experimental magnetic moments per iron atom, E^{cohe}_{exp} and E^{cohe}_{theo} are the theoretical and experimental cohesive energies, E^{f}_{exp} and E^{f}_{theo} are the theoretical and experimental energies of formation. * *Present work (LDA) and present work* show the results obtained using the von Barth Hedin local spin density functional. On the other hand *present work (P-W)* shows the results obtained for the non-local Perdew and Wang approximation.

	$Fe_{50}Al_{50}$		$Fe_{75}Al_{25}$	
a_{exp} (a.u.)	5.309–5.495	[35]	10.945	
	[40–42][49][50]	[42]	10.926	
a_{theo} (a.u.)	5.330–5.398	[42]	10.8	
	[18][19][25][40][36]			
present work (LDA)	5.37		10.65	
present work (P-W)	5.49		11.00	
B_{exp} (Gpa)	[49] 152			
	[25] 150			
B_{theo} (Gpa)	190–205			
	[19][20][40][36]			
present work (LDA)	200		176	
present work (P-W)	171		162	
μ_{exp} (μ_B)	[19] 0	[51]	$\mu_{Fe1} = 1.46$ $\mu_{Fe} = 2.14$	
μ_{theo} (μ_B)	0.69–0.71	[44]	$\mu_{Fe1} = 1.9$ $\mu_{Fe} = 2.25$	
	[19][40][44]			
present work (LDA)	0.64		$\mu_{Fe1} = 1.63$ $\mu_{Fe} = 2.23$	
present work (P-W)	0.76		$\mu_{Fe1} = 2.05$ $\mu_{Fe} = 2.48$	
E^{cohe}_{exp} (eV)	[49] –3.58			
E^{cohe}_{theo} (eV)	[19] 7.66			
	[36] –5.91			
present work	–5.90		–7.62	
E^{f}_{exp} (eV)	[52] –0.26			
	[53] –0.33			
E^{f}_{theo} (eV)	$-0.32 - -0.51$	[25]	–0.22	
	[19][21][54]			
present work	–0.46		–0.25	

If we take a closer look at the density of states *versus* energy, for this structure and composition the minority and majority spin sub-bands are very similar, they show two peaks separated by a large gap (see Fig. 3a). For small lattice parameters both sub-bands are identical in shape and occupation and the main peak is not completely full. However, as the lattice parameter increases, owing to the decrease of the hybridisation, there is a charge transfer from the minority to the majority spin sub-band, that makes the peak of this last band fill up and the one corresponding to the minority spin sub-band empty. Therefore a magnetic moment appears.

For the D03 structure and $Fe_{50}Al_{50}$ composition a larger difference between the non-magnetic and magnetic states is obtained. For this structure and composition the spin-polarized calculations give an average magnetic moment of 1.71 μ_B (see Tab. 1). The minimum of the total energy is higher than the one obtained for the B2 structure in agreement with the fact that B2 is the equilibrium phase for this composition. In comparison to the B2 case, a larger lattice parameter of 10.936 a.u. and a lower bulk modulus of 173 Gpa are obtained.

The behaviour of the average magnetic moment with lattice parameter is completely different to the one shown previously (see Fig. 2b). It increases monotonically from 0.5 μ_B to 1.9 μ_B, without showing any jump with an increase of the lattice parameter. There are two non-equivalent Fe atoms, they have the same next-nearest-neighbour environment (4 Al and 4 Fe atoms) and they show also a continuous increase of the magnetic moment with lattice parameter. This behaviour can be explained in taking into account the density of states, which is completely different to the one shown above (see Fig. 3b). In this case the majority-spin sub-band is almost full, even for low lattice parameters, and the Fermi energy is in the gap of the minority sub-band. As in the previous case, the lattice-parameter change causes a change in the hybridisation of the *sp*-Al and *d*-Fe majority and

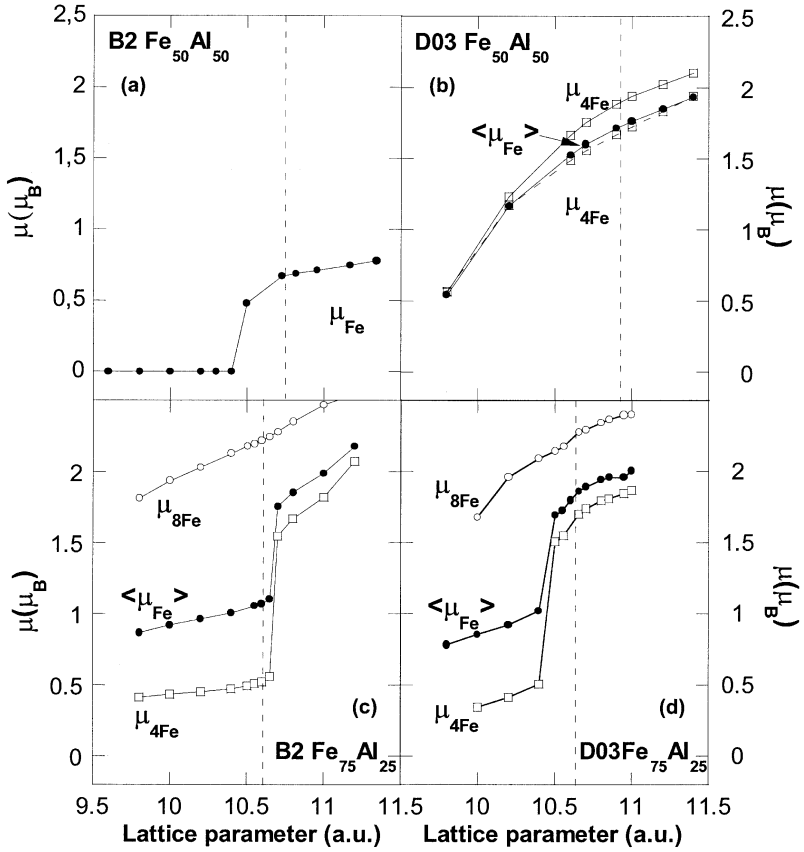

Fig. 2. Evolution of the mean magnetic moment (μ_{Fe}) and the magnetic moment for each non-equivalent Fe atom ($\mu_{4\mathrm{Fe}}$ refers to Fe atoms surrounded by 4 Fe atoms and $\mu_{8\mathrm{Fe}}$ refers to Fe atoms surrounded by 8 Fe atoms) with the lattice parameter for a) B2 $Fe_{50}Al_{50}$; b) D03 $Fe_{50}Al_{50}$; c) B2 $Fe_{75}Al_{25}$; and d) D03 $Fe_{75}Al_{25}$. For the last two structures, $\mu_{8\mathrm{Fe}}$ corresponds to the Fe2-site and $\mu_{4\mathrm{Fe}}$ corresponds to the Fe1-site in text.

minority-spin sub-bands that induces a charge transfer between the minority-spin sub-band and the majority spin sub-band that makes the magnetic moment increase with lattice parameter. However, the majority spin sub-band being almost full also for low lattice parameters, the changes induced in the magnetic moment will be small.

Andersen *et al.* [39], taking into account the generalised Stoner condition (from which it is understood that the magnetisation depends crucially on the crystal structure, the shape of the DOS, and the lattice constant), studied the change of magnetism with atomic volume for different Fe structures. They showed that depending on the structure the behaviour was different. They studied the different behaviour in Fe BCC and Fe FCC. Their results have been compared with the behaviour of the magnetic moment of Fe atoms in two different structures shown in this work. The comparison indicates that in the D03 structure, both Fe non-equivalent atoms (surrounded by 4Fe and 4Al atoms) behave like Fe-BCC, always showing a magnetic moment which changes slowly with lattice parameter. On the other hand, the Fe in the B2 structure (surrounded by 8 Al atoms) behaves like Fe-FCC that shows a large jump in the magnetic moment with the lattice parameter. Taking these results into account we can say that the different results obtained for the two different structures depend on the nearest neighbourhood of each Fe atom.

Table 3. TBLMTO bandwidth parameter Δ of Fe d-orbitals for B2 and D03 structures of $Fe_{50}Al_{50}$ and $Fe_{75}Al_{25}$ compositions. $\uparrow$ and $\downarrow$ correspond to majority and minority spin sub-bands, respectively.

Composition	Structure	a (a.u.)	Δ (eV)			
			$\uparrow$	Fe_1 $\downarrow$	$\uparrow$	Fe_2 $\downarrow$
$Fe_{50}Al_{50}$	B2	10	0.31	0.31		
		11.3	0.16	0.18		
	D03	10.2	0.26	0.29	0.26	0.30
		11.2	0.16	0.20	0.16	0.20
$Fe_{75}Al_{25}$	B2	10.2	0.26	0.27	0.24	0.29
		11.2	0.20	0.16	0.20	0.15
	D03	10.2	0.24	0.29	0.26	0.27
		11	0.18	0.22	0.18	0.22

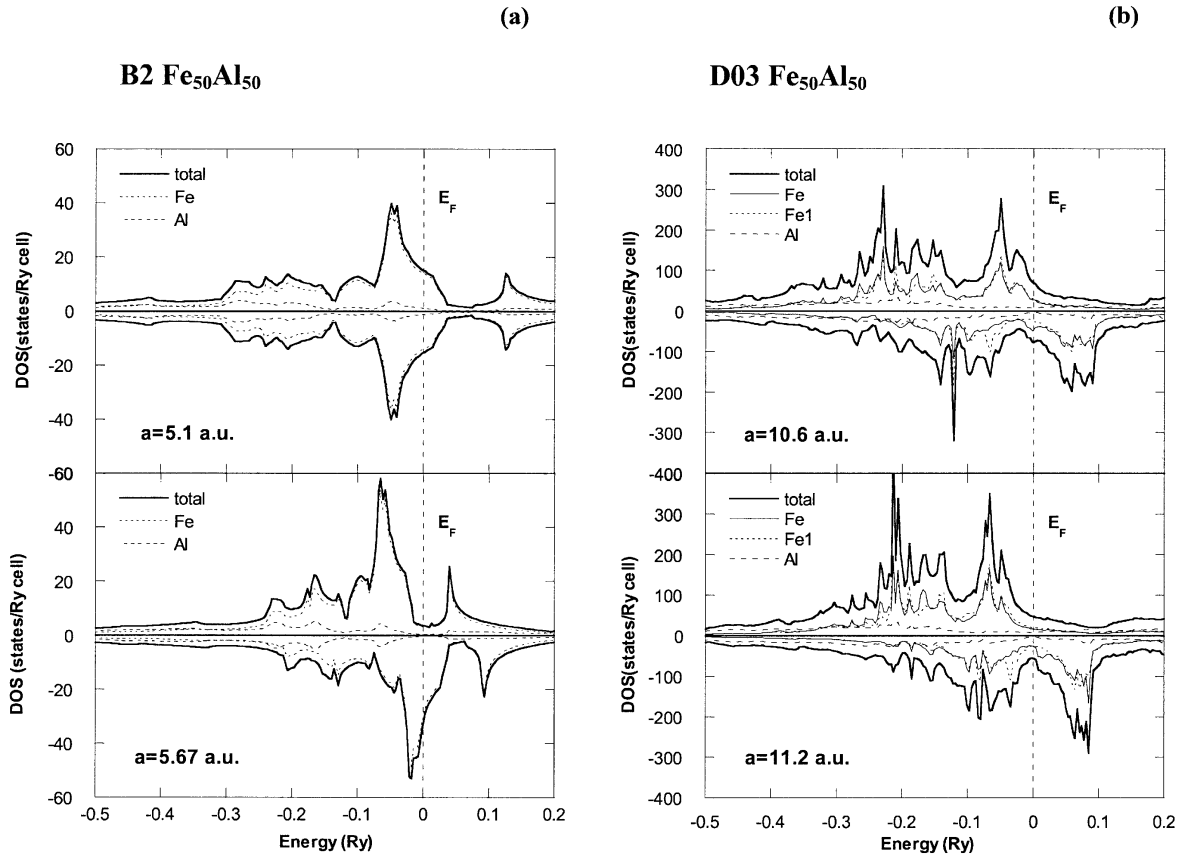

Fig. 3. Total and partial density of states for 2 different lattice parameters (above and below the equilibrium lattice parameter) for the $Fe_{50}Al_{50}$ composition in: a) B2 structure; and b) D03 structure. Fe and Fe1 are the two non-equivalent Fe atoms, both having 4 Fe atoms as nearest neighbours.

For the B32 structure, the spin polarized calculations show lower energy than the non-spin polarized ones. The spin-polarized calculations give a mean magnetic moment of 1.67 μ_B that increases monotonically with lattice parameter. As in the previous structure it does not show any jump. We obtained an equilibrium lattice parameter of 10.91 a.u. and a bulk modulus of 44 Gpa. This very low bulk modulus is related to the fact that this structure does not exist for the studied composition, and it indicates that the compositions of existence of this structure are far from $Fe_{50}Al_{50}$.

For $Fe_{50}Al_{50}$ composition the structure that shows the lower energy at the equilibrium volume is the B2 one in agreement with the phase diagram of this system [2]. On the other hand, the bulk modulus calculated for the D03 structure is closer to the experimental value than the one obtained using the B2 structure. This might indicate that the stable structure should be the D03 one [40]. However the comparison with the phase diagram indicates that the more reliable parameter is the energy minimum of each structure. It has also been discussed that for this composition and for the B2 structure the present calculations are in good agreement with previous ones, but disagree with the experimental results that show that this $Fe_{50}Al_{50}$ alloy is non-magnetic.

3.1.2 $Fe_{75}Al_{25}$

The spin-polarised calculations show a lower energy at the equilibrium volume than the non-polarised ones. In Table 1 the equilibrium lattice parameter and the minimum energy for spin-polarized and non-polarized calculations are shown. For this composition the DO3 structure is the stoichiometric one. The spin-polarised calculations show an equilibrium lattice parameter of 10.65 a.u., a value which underestimates by less than 3% the experimental values [41,42] (see Tab. 2). The bulk modulus obtained is 176 Gpa, but no experimental bulk modulus has been found in the literature. The formation energy we obtained, -0.25 eV (see Tab. 2), is in good agreement with -0.22 obtained by Kulikov *et al.* [25] for this composition. As far as the magnetic moment is concerned the calculated values for the two non-equivalent positions of the iron atoms are close to the experimental ones (see Tab. 2).

Figures 2c and d show the behaviour of the magnetic moment *versus* lattice parameter for two non-equivalent Fe atoms of DO3 and B2 structures, which in both structures have the same nearest neighbour environment: Fe1-site surrounded by 4 Fe and 4 Al atoms (μ_4 in Figs. 1c and d) and Fe2-site surrounded by 8 Fe atoms (μ_8 in Figs. 1c and d), resembling a 9 Fe-atom cluster. The behaviour of each of the Fe magnetic moments with

lattice parameter is different and once again can be compared with the different behaviours obtained for FCC and BCC iron by Andersen *et al.* [39]. The Fe1-site shows a jump above 1 μ_B in its local magnetic moment. However, the Fe located in the Fe2-site does not show any jump and its magnetic moment increases steadily with lattice-parameter increase. Therefore, the Fe mean magnetic moment shows also a jump that in the case of the DO3 structure occurs below the equilibrium lattice parameter (mean magnetic moment of 1.86 μ_B at equilibrium lattice parameter) and on the contrary, in the case of the B2 structure occurs above it (mean magnetic moment of 1.07 μ_B at equilibrium lattice parameter).

The large change in the DOS (see Fig. 4) of the Fe1-site of the two extreme lattice parameters, explains the jump in the magnetic moment that is seen in Figures 1c and d. The details of this behaviour will be discussed following the DOS of the simulated B2 structures of $Fe_{75}Al_{25}$ composition, which is similar to D03 ($Fe_{75}Al_{25}$) but easier to follow (Fig. 4). Owing to the increase of lattice parameter there is a decrease of the hybridisation (shown by the bandwidth parameter Δ in Tab. 3) and therefore a charge transfer from the minority to the majority spin sub-bands. For lattice parameters lower or equal to the equilibrium one the outermost narrow subpeak is completely empty and with the increase of the lattice parameter it fills up almost completely (the majority spin sub-band), while the minority spin sub-band empties. This makes the difference between the two sub-bands increase and therefore the magnetic moment increases abruptly.

For the Fe2-site the DOS shows that the main peaks of the local majority-spin sub-band are already full for low lattice parameters, while there is a very small contribution at the position of the outermost narrow sub-peak that is empty. There is only a small charge transfer from the minority to the majority spin sub-bands and therefore the magnetic moment increases monotonically.

For the B32 structure and this composition a lattice parameter of 10.71 a.u. and a bulk modulus of 190 Gpa are obtained. Opposite to what is found in the $Fe_{50}Al_{50}$ composition, the bulk modulus for this structure and composition is close to the values obtained for the B2 and D03 structures. This is an indication that the B32 structure may exist at large Fe contents of these alloys' series. A mean magnetic moment per Fe atom of 1.97 μ_B has been obtained. There are 3 non-equivalent Fe atoms and they all have the same next-nearest-neighbour environment (6 Fe and 2 Al atoms), their magnetic moments at the equilibrium volume go from 1.85 μ_B to 2.08 μ_B and their behaviour with lattice-parameter increase is very similar. There is no jump in the evolution of the magnetic moment with the lattice parameter. The DOS shows that the majority-spin sub-band is almost full (high value of the magnetic moment) and therefore there is only a slight change in the density of states with lattice parameter owing to the change in hybridisation and therefore of the charge transfer from the minority to the majority spin sub-band.

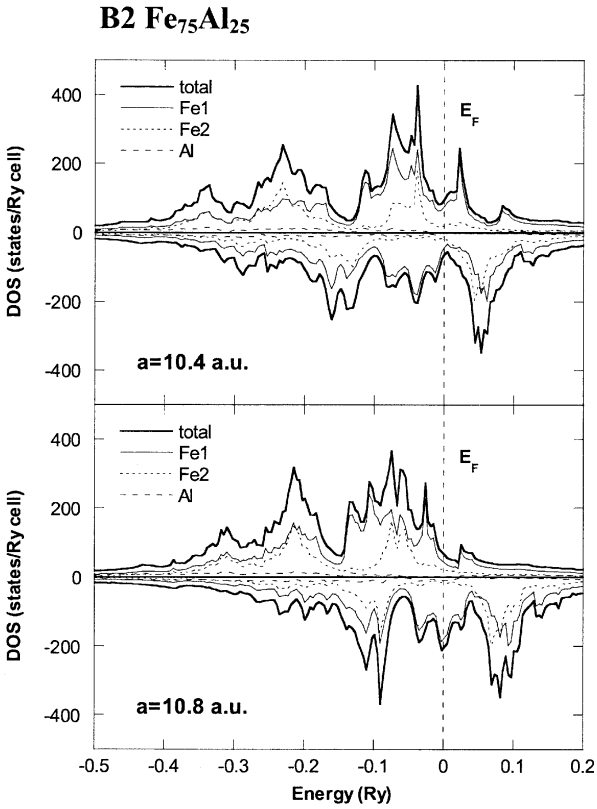

Fig. 4. Total and partial density of states for 2 different lattice parameters (above and below the equilibrium lattice parameter) for the $Fe_{75}Al_{25}$ composition in the B2 structure. Fe1 and Fe2 correspond to the Fe1-site and the Fe2-site in the text respectively. Fe2 has 8 Fe atoms as nearest neighbours and Fe1 is surrounded by 4 Fe and 4 Al atoms.

3.1.3 Higher Fe compositions

Two different concentrations in the Fe-richest side of the phase diagram were chosen and two cells that fulfil the DO3 and B32 structures conditions were built. In this case, as one is far from the range of the B2 phase existence, no calculations have been performed for it.

The energy obtained with the spin-polarised calculations is lower than the one obtained for the non-polarized calculations. Therefore we can conclude that for these structures and compositions these alloys are magnetic. For the D03 structure and $Fe_{81.25}Al_{18.75}$ concentration ($Fe_{13}Al_3$) the spin-polarised calculations show an equilibrium lattice parameter of 10.63 a.u. and a bulk modulus of 197 Gpa (see Tab. 1). In this case there are 4 non-equivalent Fe atoms, 3 of which are surrounded by 8 Fe atoms as nearest neighbours (Fe1, Fe2 and Fe3-sites) while the 4th one is surrounded by 5 Fe and 3 Al atoms (Fe4-site). There is a jump of the magnetic moment for the Fe4-site, while the magnetic moments of the other non-equivalent atoms (Fe1, Fe2 and Fe3-sites) grow steadily with lattice parameter. This can be explained by the dependence of the local DOS on the lattice parameter: the majority-spin sub-bands of the atoms surrounded by 8 Fe atoms (Fe1, Fe2 and Fe3-sites) are nearly full for

low lattice parameters, so the magnetic moment is quite high. With lattice-parameter increase, the hybridisation changes, and there is a small charge transfer from minority to the majority spin sub-band. This causes the majority-spin sub-band to fill completely and therefore the magnetic moment increases steadily. On the other hand, the Fe1-site (Fe4 site) majority-spin sub-band is not full for low lattice parameters but it fills up completely with the increase of the lattice parameter that causes the jump in the evolution of the magnetic moment.

As shown in Table 1 for the B32 and $Fe_{87.5}Al_{12.5}$ composition we obtained a lattice parameter of 10.62 a.u. and a bulk modulus of 208 Gpa (in this case this result is also relatively close to the value obtained for the D03 structure). All the Fe atoms are surrounded by 7 Fe and 1 Al atoms, therefore they show a very high magnetic moment. The values of the magnetic moment go from 2.05 μ_B to 2.24 μ_B. These high values can be explained by the shape of the density of states, where the majority-spin sub-bands are almost full for all the non-equivalent atoms. With lattice-parameter increase the magnetic moments of each non-equivalent atom change monotonically due to a small change transfer from the minority to the majority spin sub-bands.

Summarising, the calculations indicate that for B2 structure and $Fe_{50}Al_{50}$ composition the stable structure is the stoichiometric one and this is in agreement with the phase diagram [2] that shows this phase for the $Fe_{50}Al_{50}$ composition. For $Fe_{75}Al_{25}$ composition, the D03 and B2 structures show the lowest energy and this is in agreement with experimental data that shows that these two phases can coexist in the neighbourhood of this composition. The B32 structure shows the largest lattice parameter and the largest mean magnetic moment per Fe atom.

From the analysed structures it can be concluded that the shape of the DOS has a really large importance in the behaviour of the magnetic moment. When the majority-spin sub-band is completely full the magnetic moment is high. The change in the lattice parameter (inter-atomic distance) induces a change in the hybridisation and therefore a charge transfer between the majority and the minority spin sub-bands; this causes a change in the difference between the number of occupied states in the sub-bands, which will cause the magnetic moment to change.

The behaviour of the magnetic moment is different depending on the environment of the iron atoms. It is interesting to notice that the behaviour of the non-equivalent Fe with lattice parameter is quite similar when they have similar environments independently of the structure under which the calculations are performed. The calculations indicate that the number of Fe atoms in the nearest neighbourhood of one Fe atom which are needed to cause an abrupt jump of its magnetic moment (with lattice-parameter variation) increases as the Fe content increases in the alloy. This is a clear indication that the position of the peak of the DOS corresponding to the *d*-Fe orbital of that environment moves to larger energies (relative to the Fermi energy) as the iron-content increase.

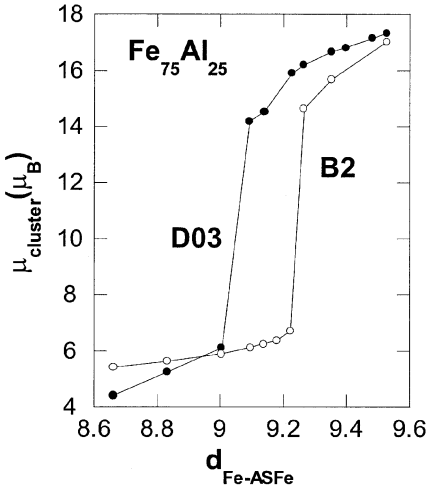

Fig. 5. Evolution of the magnetic moment of a 9-Fe atom-cluster with the ASFe-Fe distance for the $Fe_{75}Al_{25}$ composition and two different structures (D03, B2).

Table 1 indicates that the equilibrium lattice parameter decreases with the Fe content increase in the alloy. In addition, as can be expected, the magnetic moment increases with Fe content.

Moruzzi *et al.* [43] classified the paramagnetic to ferromagnetic transitions taking into account the evolution of the magnetic moment with volume. Comparing this classification with the results obtained in this work, it can be said that the B2 $Fe_{50}Al_{50}$ alloys have a type I transition. However, for all the structures and compositions the scanned volume is not sufficient to reach the onset and therefore no type can be assigned to them.

3.2 Fe-clusters

Fe2-sites in the DO3 and B2 structures of $Fe_{75}Al_{25}$ can be compared to 9 Fe-atom cluster calculations found in the literature [21,44], where the Fe2-site corresponds to the antisite (AS) Fe atom (μ_{8Fe} in Figs. 2c and d). These types of clusters may be present in the samples and might be the cause of the discrepancy in the magnetic moment between theory and experiments in the $Fe_{50}Al_{50}$ stoichiometric alloy [44]. The calculations in the literature [21,44] were performed for interatomic Fe-Fe distances that correspond to the experimental lattice parameter of the FeAl composition.

The results obtained in this work depend on the cell structure we are analysing. For B2 ($Fe_{75}Al_{25}$), taking the value corresponding to the theoretical equilibrium lattice parameter, a magnetic moment of 6.4 μ_B was obtained (2.2 μ_B for the antisite (AS) Fe atom and 0.52 μ_B for the 8 surrounding atoms). Moreover, the cluster results at the equilibrium lattice parameter for D03 ($Fe_{75}Al_{25}$) give a magnetic moment of 15.24 μ_B (2.2 μ_B for the antisite (AS) Fe atom and 1.6 μ_B for the surrounding atoms), much larger than in the previous case. It is interesting

to notice that the AS-Fe magnetic moment at the equilibrium lattice parameter is 2.2 μ_B independently of the structure under which the calculations were performed. The trend of the magnetic moments of different Fe atoms in both clusters are similar and Figure 5 indicates that there is a shift of the magnetic moment of the cluster with respect to the ASFe-Fe distance. Figure 5 also shows that for ASFe-Fe distances shorter than 9 a.u. the magnetic moment of the clusters simulated with D03 and B2 structures in $Fe_{75}Al_{25}$ give similar magnetic moment. The magnetic moment of the AS-Fe varies slowly but the surrounding 8 atoms of the cluster have a strong dependence on ASFe-Fe distance. Indeed, in the B2 ($Fe_{75}Al_{25}$) structure, a 4% inward relaxation of the atoms surrounding the AS-Fe atom gives a cluster magnetic moment of 5.7 μ_B (1.7 μ_B for the AS-Fe atom and 0.5 μ_B for the surrounding 8 Fe-atoms) as predicted by Bogner *et al.* [44]. The same amount of inwards relaxation (4%) in the case of D03 ($Fe_{75}Al_{25}$) gives a magnetic moment of 5.26 μ_B for the cluster, in good agreement with the experimental results obtained by Bogner *et al.* [44].

As shown, the magnetic moments of the cluster obtained in this work for equilibrium lattice parameters are in between the ones of references [21] and [44]. However, the present results indicate clearly that the magnetic moments of the 9 Fe-atom clusters are very dependent on the ASFe-Fe distance.

3.3 Disordered structure (A2)

Most of the theoretical work done to study the reinforcement of magnetism in these alloys has been performed assuming point defects [21,24,45] and antiphase boundaries [47]. Recently, several articles have studied by self-consistent methods the disordered structures for compositions near the equiatomic B2 one using the Coherent Potential Approximation (CPA) [22,36]. Kulikov *et al.* [25] found magnetism in the studied range of disordered alloys but opposite to the experimental results they found a decrease of lattice parameter with disordering in all the studied composition range.

Taking into account that X-ray diffraction of severe cold deformed (mechanically milled) FeAl alloys shows diffraction peaks corresponding to the A2 structure [46,48], and that this structure also appears in samples prepared by rapid quenching from the melt [47,48], we have simulated the disorder in FeAl alloys by means of the A2 structure. On the other hand, the magnetic properties depend strongly on the local environment, which at the same time depends on the chosen cell. In order to make a good approximation, the average of seven different A2 supercells for $Fe_{50}Al_{50}$ composition and seven different A2 supercells for $Fe_{75}Al_{25}$ composition have been used to compare theoretical and experimental results.

Table 1 shows the average of the minimum energy of the studied A2 disordered structures for spin-polarized and unpolarized calculations. The spin-polarised calculations have a lower energy than the unpolarised ones and therefore we can conclude that for these structures and compositions these alloys are magnetic in all the different cells built, independently of the Fe content ($Fe_{50}Al_{50}$ or $Fe_{75}Al_{25}$). Table 1 also shows that the equilibrium lattice parameter decreases with Fe-content increase in the alloy. The mean lattice parameter for the A2-$Fe_{50}Al_{50}$ composition is 10.95(0.02) a.u. and 10.72(0.01) a.u for the $Fe_{75}Al_{25}$ composition. These values underestimate by less than 3% the experimental value obtained by Frommeyer *et al.* [35] in deformed or ball milled samples of $Fe_{70}Al_{30}$ that present the A2 structure. It is worth mentioning that this underestimate is of the same order as the one found between the $Fe_{75}Al_{25}$ D03 ordered theoretical and experimental values.

The mean magnetic moment at the equilibrium volume is 1.7(0.1) μ_B for $Fe_{50}Al_{50}$ and for $Fe_{75}Al_{25}$ 2.00(0.06) μ_B.

3.4 Comparison between ordered and disordered structures

The equilibrium lattice parameter of the calculated A2 structures is larger than the corresponding ordered (B2 and DO3) ones (see Tab. 1), in good agreement with X-ray diffraction observations after severe deformation in alloys of similar composition [14]. These results are in very good agreement with the lattice-parameter increase in deformation experiments. However, it disagrees with the calculations performed under the KKR-CPA approach [25]. Moreover, it must be remarked that the theoretical increase of lattice parameter between the A2 and D03 structures of $Fe_{75}Al_{25}$ is 0.75%, in very good agreement with the experimental increase after deformation of about 0.7% found both for $Fe_{70}Al_{30}$ [35] and $Fe_{60}Al_{40}$ [14]. In the case of $Fe_{50}Al_{50}$ the increase of lattice parameter with disorder is 2%. Therefore, the results obtained are in good agreement with the experimental ones.

The magnetic moment per iron atom increases with disorder (see Tab. 1). This is specially pronounced in the case of $Fe_{50}Al_{50}$ (B2), where the magnetic moment increases in more than 1 μ_B after disordering. These theoretical results are in agreement with the experimentally observed increase of magnetism in deformed or ball-milled alloys [15] that, as previously cited, also show an increase in the lattice parameter with any type of deformation.

Figure 6 shows the density of states with respect to the energy for an ordered and a disordered structure of $Fe_{50}Al_{50}$ composition. Owing to the lower lattice parameter of the B2 alloy, the hybridisation of the *sp*- and *d*-bands is larger than for the disordered structure (higher Δ parameters) and therefore the difference between the two bands is larger in the disordered case which causes the magnetic moment to be higher. In addition to this, the nearest neighbour configuration of each iron atom (in the disordered structure not every iron atom is surrounded by 8 Al atoms, as it happens in B2 $Fe_{50}Al_{50}$) favours a larger magnetic moment. In the same Figure 6 we can see that the major contribution is given by the iron atom and, as in previous cases, this contribution comes mainly from the *d*-band.

Hernando *et al.* [15] have found that an important contribution to the magnetism of these alloys comes from

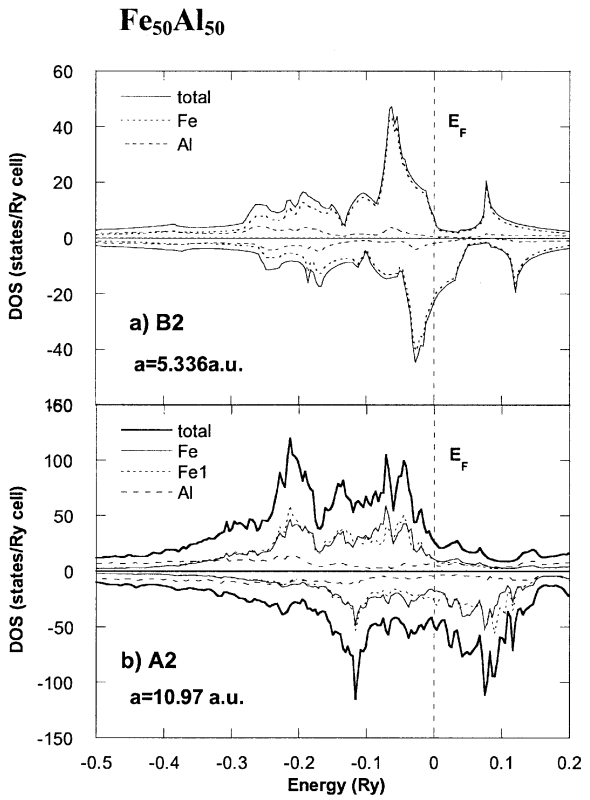

Fig. 6. Total and partial density of states at the equilibrium volume for the $Fe_{50}Al_{50}$ composition a) B2 structure, and b) A2 structure.

changes in the lattice parameter induced by the order-disorder transition. This contribution is linked to modifications in the electronic band structure induced by volume changes. In the present work, it has been clearly shown, through the study of the lattice-parameter dependence of the magnetic moment, that this effect is important all along the different structures and compositions that were studied. However, our results indicate that the disorder has also a large contribution which, depending on the composition, can be even larger than the lattice contribution.

4 Conclusions

The calculations performed on B2, D03 and B32 structures for different compositions of the Fe-rich side of the Fe-Al system show results that are in good agreement with the scarce experimental data available in the literature.

The too low bulk modulus calculated in the B32 structure for $Fe_{50}Al_{50}$ clearly indicates that this structure cannot exist at concentrations close to $Fe_{50}Al_{50}$.

The calculations show a large dependence of the magnetic moment with the lattice parameter in all the studied structures and compositions. The hybridisation of the majority and minority spin Fe *d*-orbitals with its neighbours changes significantly with the lattice parameter as seen in the values of the LMTO band-width parameter Δ for Fe *d*-orbitals. This hybridisation causes charge transfer between both majority and minority spin sub-bands and therefore a change in the magnetic moment.

For $Fe_{50}Al_{50}$ and $Fe_{75}Al_{25}$ compositions, at the energy minimum, the D03 structure shows both larger magnetic moment and larger lattice parameter than the B2 structure. The calculations indicate clearly that the magnetic moment of nine Fe-atom clusters is very dependent on the ASFe-Fe distance, so the comparison with experiment is not straightforward.

The comparison between calculations performed in ordered and disordered structures of the same composition indicates that the disorder makes both the lattice parameter and the magnetism increase in comparison to the ordered structures. Indeed, the lattice parameter increase with disorder for $Fe_{50}Al_{50}$ and $Fe_{75}Al_{25}$ alloys is in good agreement with experimental results. The contribution of disorder to the magnetism of these alloys can be even larger that the contribution of the lattice-parameter increase.

This work has been undertaken under projects No. PB98-0780-CO2 (DGICYT, Spain), MAT2002-4087-C02-01, UPV 224.310-EB153 and UPV 224.310-14553/2002. One of us (E.A.) would like to thank the Basque Government for financial support. The authors are very much indebted to O.K. Andersen and O. Jepsen for supplying the TB-LMTO code and to the members of Andersen's Department (Max Planck Institute for Solid State Physics, Stuttgart) for their helpful comments.

References

1. E.P. Wohlfath, K.H.J. Buschow, *Handbook of Ferromagnetic Materials* (North Holland Elvier Science Publishers, Amsterdam, New York, Oxford, Tokio, 1988), Vol. 4, Chap. 1
2. O. Kubaschewski, *Iron Binary Phase Diagrams* (Springer, Berlin, 1986)
3. M. Becker, W. Schweike, Scripta Materialia **35**, 11 (1996)
4. W. Schweika, *Materials Research Society Symposium Proceedings*, Vol. 166 (1990), p. 249
5. E. Jartych, J. Zurawicz, D. Oleszak, M. Pekala, J. Sarzynski, Mieczyshan, M. Budzynski, J. Magn. Mag. Mater. **186**, 3 (1998)
6. M.J. Besnus, A. Herr, A.J.P. Meyer, J. Phys. F **5**, 2138 (1975)
7. D.A. Eelman, J.R. Dahn, G.R. Macklay, R.A. Dunlap, J. Alloys, Compounds **266**, 1 (1998)
8. P.A. Beck, Met. Trans. **2**, 2051 (1971)
9. L. Hedin, B.I. Lundqvist, J. Phys. C **4**, 2064 (1971)
10. P. Huffman, R.M. Fisher, J. Appl. Phys. **38**, 735 (1967)
11. A. Taylor, R.M. Jones, J. Phys. Chem. Solids **6**, 16 (1958)
12. A. Arrot, H. Sato, Phys. Rev. **114**, 1420 (1959)
13. I. Vincze, Phys. Stat. Sol. (a) **7**, K43 (1971)
14. S. Surinach, X. Amils, S. Gionelle, L. Lutterotti, M.D. Baró, Mat. Sci. Forum **235**, 228 (1997)
15. H. Hernando, X. Amils, J. Nogués, S. Suriñach, M.D. Baró, M.K. Ibarra, Phys. Rev. B **58**, R 11864 (1998)
16. A. Hernando, J.M. Rojo, J.C. Gomez-Sal, J.M. Novo, J. App. Physics **79**, 4815 (1996)
17. J.H. Westbrook, R.L. Fleischer, *Intermetallic Compounds*, Vol. 1 (Wiley Chicester, 1994), p. 127

18. R.E. Watson, M. Weinert, Phys. Rev. B **58**, 5981 (1998)
19. V. Sundararajan, B.R. Sahu, D.G. Kanhere, P.V. Panat, G.P. Das, J. Phys. Cond. Matt. **7**, 6019 (1995)
20. R. Haydock, M.V. You, Solid State Comm. **33**, 299 (1980)
21. Y.M. Gu, L. Fritsche, J. Phys. Cond. Matt. **4**, 1905 (1992)
22. S.K. Bose, V. Drchal, J. Kudrnovsky, O. Jepsen, O.K. Andersen, Phys. Rev. B **55**, 8184 (1997)
23. W. Lin, Jian-hua Xu, A.J. Freeman, J. Mater. Res. **7**, 592 (1992)
24. C.L. Fu, Phys. Rev. B **52**, 315 (1995)
25. N.I. Kulikov, A.V. Postkikov, G. Borstel, J. Braun, Phys. Rev. B **59**, 6824 (1999)
26. O.K. Andersen, Phys. Rev. B **12**, 3060 (1975)
27. H.L. Skriver, *The LMTO Method* (Springer-Verlag, Berlin Heidelberg 1984)
28. O.K. Andersen, O. Jepsen, Phys. Rev. Lett. **53**, 2571 (1984)
29. U. Von Barth, L. Hendin, J. Phys. C **5**, 1639 (1972)
30. P. Bagno, O. Jepsen, O. Gunnarsson, Phys. Rev. B **40**, 1997 (1989)
31. F.D. Murnaghan, Proc. Natl. Acad. Sci. **30** (1944)
32. O. Jepsen, O.K. Andersen, Solid State Commun. **8**, 1763 (1971)
33. O.K. Andersen, O. Jepsen, Phys. Rev. B **49**, 5965 (1994)
34. F. Schmidt, K. Binder, J. Phy. Cond. Matt. **4**, 3569 (1992)
35. G. Frommeyer, J.A. Jimenez, C. Derder, Z. Metallkd. **90**, 43 (1999)
36. J. Mayer, C. Elsässer, M. Fähnle, Phys. Stat. Sol. (b) **191**, 283 (1995)
37. V. Heine, Phys. Rev. **153**, 673 (1967)
38. O. Gunnarsson, O. Jepsen, O.K. Andersen, Phys. Rev. B **27**, 7144 (1983)
39. O.K. Andersen, O. Jepsen, D. Glötzel, *Highlights of Condensed-Matter Theory: Canonical Description of the Band Structure of Metals* (Soc. Italiana di Fisica-Bologna, 1985), p. 155
40. V.L. Moruzzi, P.M. Marcus, Phys. Rev. B **46**, 2864 (1993)
41. R. Kuentzler, J. Phys. France **44**, 1163 (1983)
42. S. Dorfman, V. Liubich, D. Fuks, Inter. J. Quantum Quem. **75**, 4 (1999)
43. V.L. Moruzzi, Phys. Rev. Lett. **57**, 2211 (1986)
44. J. Bogner, W. Steiner, M. Rissner, P. Mohn, P. Blaha, K. Schwarz, R. Krachler, H. Ipser, B. Sepiol, Phys. Rew. B **58**, 22 (1998)
45. G. Bester, B. Meyer, M. Fähnle, Phys. Rev. B **60**, 14492 (1999)
46. B. Fultz, Z. Gao, Phil. Mag. B **67**, 6 (1993)
47. N.A. Dubrovinskaia, L.S. Dubrovinsky, A. Karlsson, S.K. Saxena, B. Sundaman, Calphad **23**, 1 (1999)
48. D. Rafaja, Scripta Mat. **34**, 9 (1996)
49. P.A. Schultz, J.W. Davenport, Scripta Metall. **27**, 629 (1992)
50. C. Müller, W. Blau, P. Ziesche, Phil. Stat. Sol. (b) **116**, 561 (1983)
51. R. Nathans, H.T. Pigott, C.G. Shull, J. Phys. Solids **6**, 38 (1958)
52. P. Villars, L.D. Calvert, *Pearson's Handbook of Crystallographic Data for Intermetallic Phases*, Vols. 1–3 (Metals Park, OH: American Society for Metals, 1985)
53. F.R. de Boer, R. Boom, W.C. Mattens, A.R. Miedema, A.K. Niesen, *Cohesion Metals: Transition Metal Alloys* (North-Holland, Amsterdam, 1988)
54. J. Zou, C.L. Fu, Phys. Rev. B **51**, 4 (1995)